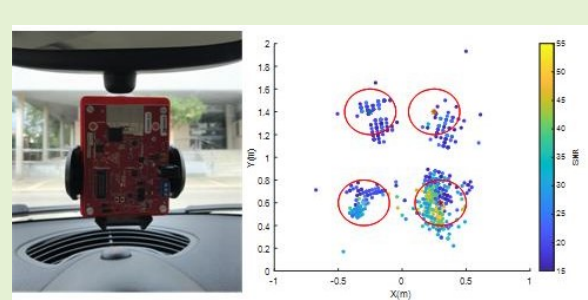


# Vehicle occupancy detector based on FMCW mm-wave radar at 77 GHz

N. Munte, A. Lazaro, *Senior, IEEE*, R. Villarino, D. Girbau, *Senior, IEEE*

**Abstract**— Millimeter-wave (mmWave) radars are a solution in automotive applications such as Adaptive Driver Assisted Systems (ADAS). This work explores the use of commercially-available mmWave radar technology for in-cab vehicle applications. A framework for vehicle occupancy detector based on mmWave radar at 77 GHz is presented. A multiple-input multiple-output (MIMO) frequency-modulated continuous wave (FMCW) radar from Texas Instruments (AWR1642) is used. The system can detect the presence of people occupying the seats by measuring small movements of the body. To this end, the static clutter is removed, therefore the point cloud returned by the radar contains information about the body. The radar is installed on the roof of the vehicle to have the maximum field of view of the seats. An algorithm that uses both the density and the dispersion of points around each seat is proposed to determine its degree of occupation. Experimental results have been presented for 4 and 5-seater vehicles with high accuracy.

**Index Terms**— Automotive radar, mm-wave radar, seat occupancy, detection, V2X



## I. INTRODUCTION

ELECTRONIC systems used to detect, identify and count occupants within a vehicle are referred to as vehicle occupancy detection systems. Their use is rising since they can help in the mobility field in topics such as decreasing traffic congestion, saving time and reducing environmental pollution.

Traffic congestion is rising and becoming a serious issue in most of the cities. It is created by an increase in the number of vehicles on the road, which results in slower speeds, road blockages, longer travel times, wasting valuable time and negatively impacting the economy.

High-occupancy-vehicle (HOV) lanes are being promoted by government regulations as a new strategy to increase road and city mobility. HOV lanes will serve to alleviate general congestion by encouraging the usage of carpooling, public transportation and transit. HOV lanes and congestion toll discount policies are in place to promote vehicle sharing. However, vehicle occupancy detection, needed to implement such policies, is often done using labor-intensive manual procedures [1]. Increasingly, access to congested cities and places is being gradually restricted, taking into account environmental criteria. As a result, the demand for vehicle occupancy detection

Manuscript received December 20, 2021; accepted January xx, 2022. Date of publication January xx, 2022; date of current version January xx, 2022. This work was supported by the Spanish Government Project RTI2018-096019-B-C31, the R2B2020 project and the EU's European Regional Development Fund (ERDF).

The authors are with the Electronics, Electrical and Automatics Engineering Department, Rovira and Virgili University, Tarragona, Spain (e-mail: nil.munte@urv.cat, antonioramon.lazaro@urv.cat, ramon.villarino@urv.cat, david.girbau@urv.cat). The corresponding author is A. Lazaro (e-mail: antonioramon.lazaro@urv.cat).

systems is expected to rise in the coming years.

Radar technology can identify the presence of a person even in the most difficult of environments, such as in bad weather conditions, or in the presence of intense light or darkness. Millimeter waves, unlike other sensing technologies, can pass through materials like plastic and clothing. In this way, sensors can be hidden behind a housing or placed inside or beneath other components of the car, thus being non-contact and non-intrusive. An ultrasonic sensor, for example, cannot distinguish the difference between a human and a static object, and cameras will not detect a baby in bright or dark light conditions. Recently, the authors have proposed a seat-occupancy detector and breathing monitoring based on a low-cost coherent-pulsed mmWave radar at 60 GHz. However, due to its short-range (on the order of 1 meter), a radar sensor must be installed in front of each seat [2]. This study proposes a different solution that overcomes those limits. It proposes a FMCW MIMO radar operating at the 77 GHz band to determine the degree of occupancy of vehicles with multiple passengers.

The paper is organized as follows. After the introduction, in section II, different systems proposed to detect occupants inside a vehicle are reviewed. Section III describes the proposed solution based on a 77 GHz mmWave radar. Experimental results and discussion are given in section IV. Finally, conclusions are provided in section V.

## II. STATE-OF-THE-ART

Several studies and companies have attempted to design an automated detection method to overcome this challenge.

Vehicle occupancy detection methods proposed in the literature are mainly based on video systems, which have different ways of classifying images [1], [3]–[9] and thermal images [10]–[13]. Recently, commercial products based on video and computer tools have been designed for these applications and marketed by suppliers providers such as Xerox, Conduent Inc., Invision AI, Fortran Traffic Systems Limited, Indra, and Siemens. However, since these products are not boarded in the car but are external, and due to various factors such as tinted windows, obstruction and variation in occupant posture, vehicle speed, size, shape, imaging geometry variation, and bad weather conditions, the vehicle passenger occupancy detection method based on video has several drawbacks in distinguishing between passengers and objects placed on the seat, which can reduce cases of successful detection. Systems based on thermal images have higher cost compared to optical video-based systems. Thus, the design of alternative cost-effective vehicle occupancy detection systems is needed to attract more customers.

The integration of detection devices inside vehicles is another option to determine their degree of occupancy. On the other hand, the use of on-board seat-occupancy detection systems is also used in other applications so, one only system could be shared by these applications. For instance, airbag systems are fundamental safety elements in modern vehicles and they require information about the presence and type of passenger who may occupy the seat to work properly. Unwanted airbag activation results in costly repair operation. Additionally, activation an airbag in a seat occupied by a rear-facing baby seat can result in fatal injuries [14]. As a result, sensors to detect seat occupancy are required, preventing the airbag from activating when the seat is not occupied by a user or by a rear-facing baby. Seat belt is another mandatory safety system. A different application of the seat occupancy detector is as a seat belt reminder. Conventional seat belt reminder systems work with weight sensors. As a result, when the seats are occupied by luggage or purchases, they generate unwanted alarms. Seat occupancy monitoring systems can also be used to improve passenger's comfort, in addition to meeting regulatory requirements, such as managing the air conditioning system based on the occupancy rate. Another use is to alert the presence of children or pets, preventing the driver from forgetting them inside the vehicle.

In the literature, various approaches to on-board detect seat occupancy have been proposed. There are two types of methods: with contact and without contact. The first approach is based on installing a sensor in the seat to detect the presence of a person, whilst the second way relies on devices that detect the presence of an occupant at a distance using electromagnetic waves or optical systems. The diagram shown in Fig.1 summarizes different seat-occupancy detection systems.

Pressure sensors is a widespread contact method to detect seat occupancy, [15] [16]. The main limitations with these sensors is their sensitivity to vibrations and that the passenger must be in contact with the seat. Another type of sensor is based on the use of capacitive sensing and consists of a set of electrode arrays embedded in the seat [17]–[19]. On the other hand, these sensors are sensitive to interference as well as the

distance between the body and the seat.

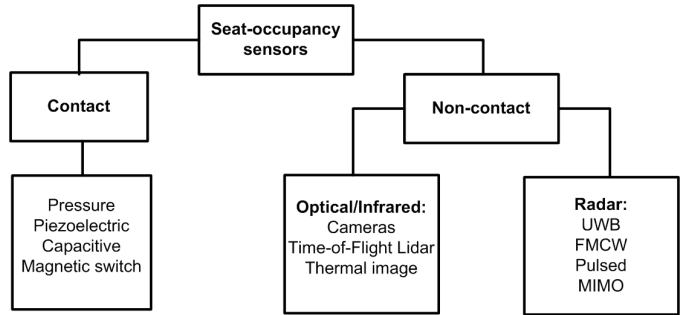


**Fig. 1.** Classification of seat-occupancy detection systems.

Recently, contactless seat-occupancy detection is gaining interest. Optical sensors, such as the use of cameras [20]–[22] could be a viable alternative as detection systems, particularly for rear-seat applications. Recently, in [22] a camera-based method to monitor breathing from a reflective object attached to the belt has been studied. The time-of-flight measured with LIDAR sensors has also been proposed as a seat-occupancy detection method [23]. The main disadvantage of camera-based systems is that they rely on face or shape detection, making it difficult to use in low-light situations or when children are dressed. Infrared cameras can detect people in low-light conditions thanks to body heat, but humans may not be distinguished when the interior of the automobile is hot, such as in summer. In addition, infrared cameras are more expensive than traditional ones. These vision systems use extensive signal processing techniques, which greatly increases the computational cost and resources that must be added to that of the system. Recent developments in new technologies such as millimeter wave (mmWave) radar sensors and V2X communications [24] can contribute to develop future vehicle occupancy detection systems. The cost of these radars is falling due to increasing mass marketing in different Advanced Driver Assistance Systems (ADAS) and the development of mmWave semiconductor devices for 5G communications systems. Radar systems applied to vehicle occupancy detection are beginning to be investigated. Car designers have already successfully integrated millimeter-wave (mmWave) sensors within the vehicle cabin for automotive applications. One of these potential applications is the ability to detect occupants within the vehicle considering a variety of both lighting conditions and sensor locations, regardless of movement. For instance, this can help automotive systems detect an unattended child in the rear of the car or the position of the occupants to control the temperature.

Recently, different radar types have been studied for vital-signs monitoring such as [25]–[27], Continuous Wave (CW) Doppler radars [28]–[30], Frequency-Modulated Continuous-Wave Radar (FMCW) Radar [31] or Impulse Radio Ultra-Wide Band (IR-UWB). However, a relatively small number of works have focused on automotive in-cabine applications. Seat occupancy based on FMCW microwave and mm-wave radars at 24 GHz and 77 GHz have been recently proposed in [32] and [33], respectively. Seat occupancy detection based on monitoring the received UWB signal has been proposed

in [34]. A system based on a coherent pulse radar at 60 GHz capable of detecting the presence of a passenger and measuring the breathing rate has been presented in [2]. This work is based on MIMO FMCW radar technology because it is able to detect small movements, as well as range and angle of several targets simultaneously. These features besides the maturity of this technology in the automotive sector, and therefore the experience of the vehicle manufacturers, making it ideal for this application over other radar technologies.

### III. SYSTEM DESIGN AND THEORETICAL BACKGROUND

#### A. System overview

The system is based on the mmWave AWR1642 radar chipset [35] from Texas Instruments (TI, Dallas, USA). It incorporates an FMCW radar that have 2 transmitters and 4 receivers with built-in phase lock loop (PLL) and analog-to-digital converters (ADC). TI's evaluation board, AWR162 BOOST [36], which also integrates a C674x digital signal processor (DSP) and an ARM R4F base-band microcontroller for the signal processing, the radar setup and communications with an external host controller, is used in this work. Fig. 2 shows a block diagram of the board. The radar can operate in the 76-77 GHz or 77-81 GHz band transmitting up to 12.5 dBm. The board implements a virtual antenna array with 8 equivalent antennas spaced  $\lambda/2$ . Each of the antennas of the array has a maximum gain of 9 dBi in the 76-81 GHz operating band.

The radar is suspended from the sunroof of the car for demonstration purposes, pointing towards the seats, as seen in Figure 3. In a real non-demonstration scenario, it will most likely be installed around the rear view mirror, or even on the ceiling. Two cases will be investigated, a 4-seater car and a 5-seater car, as shown in Figure 3. Fig. 4 shows the radar board installed on the front glass of a vehicle that was used for testing in this work.

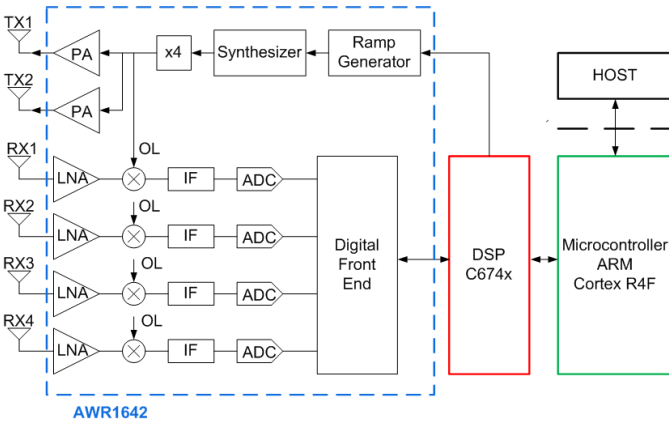


Fig. 2. TI evaluation board AWR1642 BOOST diagram.

#### B. Basic measurement theory

An FMCW radar transmits a frame composed by  $L$  chirp signals (see Fig.5). Each chirp is a signal whose frequency varies with time from the minimum value  $f_{min}$  to a maximum

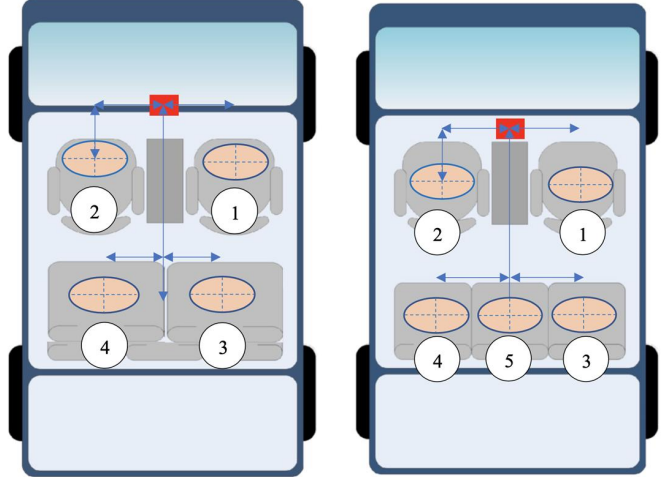


Fig. 3. Installing the radar in a 4-seat car and 5-seat car, and seat numbering.



Fig. 4. Photograph of the radar attached to the front glass for testing.

value  $f_{max}$  following the shape of a saw tooth, being  $B = f_{max} - f_{min}$ . A linear chirp signal performs a linear sweep in frequency from a specific frequency value to a higher one (or vice versa). A typical FMCW chirp signal can be written as:

$$x_c(t) = \exp(j2\pi(f_c t + \frac{\mu}{2}t^2)) \quad (1)$$

where  $f_c$  is the carrier frequency and  $\mu = B/T$  is the slope of the chirp signal, being  $T$  the sweep time. The transmitted signal is composed by  $L$  chirps and it can be expressed as:

$$x_T(t) = \sum_{l=0}^{L-1} x_c(t) \prod \left( \frac{t - lT}{T} \right) \quad (2)$$

where  $\prod(t)$  is the normalized rectangular signal. In each of the four receivers, the received signal and transmitted signals are mixed and filtered to finally obtain the beat signal, which is sampled and discretized at a rate of  $f_s$  using a fast ADC

**TABLE I**  
CONFIGURATION OF THE FMCW RADAR

Parameter	Value
Start Frequency	77 GHz
Sweep bandwidth	3.44 GHz
Sweep slope	70 MHz/ $\mu$ s
Frame duration	100 ms
Sampling frequency	5209 kbps
Number of samples per chirp	256
Number of chirps per frame	32
Transmit antennas	2
Receive antennas	4

for the post processing. The received signal of the  $k$ th array element for each  $l$ th chirp is given by [37]:

$$x_{r,lk}(t) = ax_c(t - \tau) \exp(j2\pi f_D l T) \exp(j\frac{2\pi}{\lambda}dk \sin\theta) \quad (3)$$

The beat signal obtained for the  $l$ th chirp and the  $k$ th array element  $y_{lk}(t)$  can be expressed as [37]:

$$y_{lk}(t) = x_{r,lk}(t) \cdot x_T(t)^* \quad (4)$$

$$y_{l,k}(t) = a \cdot \exp(-j(2\pi f_c \tau - \mu \tau^2/2)) \cdot \exp(-j2\pi \mu \tau t) \cdot \exp(j2\pi f_D l T) \cdot \exp(j\frac{2\pi d}{\lambda} \sin(\theta)) \quad (5)$$

where  $a$  is the amplitude of the target,  $d$  is the spacing between adjacent antenna elements,  $\lambda$  is the wavelength at the carrier frequency,  $\tau$  is the propagation delay,  $f_D$  is the Doppler frequency shift due to velocity, and  $\theta$  is the angle-of-arrival. Therefore, the first term is a complex amplitude, the second is a time-of-arrival term that depends on range, the third is the Doppler and it is related to movement, and the last term is the direction-of-arrival (DOA) that depends on the angle-of-arrival. The samples  $y_{lk}[n] = y_{lk}(nT_s)$  for  $n = 0, 1, \dots, N_s - 1$  are saved in a tridimensional matrix.

The processing chain implemented in the board DSP [38] is described in Fig. 6. A windowed Fast Fourier transform applied to the samples of each chirp (FFT in range) is used to estimate range. The resolution in range depends on the ability to discriminate the peaks of the spectrum to resolve targets. Thus, the range resolution is determined by:

$$\Delta R = \frac{c}{2B} \quad (6)$$

Considering a bandwidth of 3.4 GHz, a range resolution of 4.4 cm from (6) is obtained. The main goal of this work is to distinguish between people and inanimate objects that may be in the seats or between people and static clutter, based on the movements detected that could be as small as those associated with breathing. Thus, before of performing the 2D-FFT, a static clutter removal algorithm is implemented by subtracting the mean value of the input samples.

Subsequently, another FFT (Doppler FFT) is applied for each chirp and antenna channel, obtaining a range-Doppler map for each  $k$ th array element. In order to reduce clutter, a constant false alarm rate (CFAR) algorithm is used to estimate a threshold. Points above this threshold are considered clutter and are removed from the range-Doppler map. Several CFAR algorithms have been proposed in the literature so far [39],

[40], however in this work the cell-averaging (CA-CFAR) is used for its simplicity [41]. This algorithm estimates the surrounding noise power by averaging the neighboring cells to the cell of interest. A third FFT (AoA FFT) is then applied. The FFT-based algorithm for DOA detection is the most widely used algorithm because of its low complexity and ease of implementation [42]. The angle estimation is performed via processing the received signal at the array composed by multiple elements. The simplest algorithm is the angle FFT algorithm. If a Fourier transform is performed in the spatial dimension through the receiver elements (known as angle FFT) it will be possible to distinguish objects based on their AoA ( $\theta$ ) in azimuth. Enhanced angular algorithms can be employed such as ESPRIT [43], MUSIC [42], [44] or Capon beamformer [45]. In this work, the point cloud is used as the occupancy detection input. The total procedure requires three fast Fourier transforms (in range, velocity and angle) as shown in Fig. 6. On the radar sensor board, preliminary processing of the signal received by the radar is performed, yielding a point cloud. The board provides a signal-to-noise ratio (SNR) for each point estimated from the previously saved noise profile. The point cloud is then processed on a Raspberry Pi 4 or a personal computer.

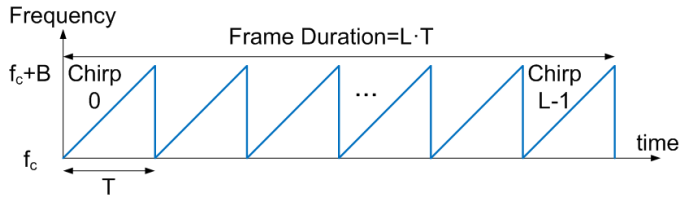


Fig. 5. Frame of chirps.

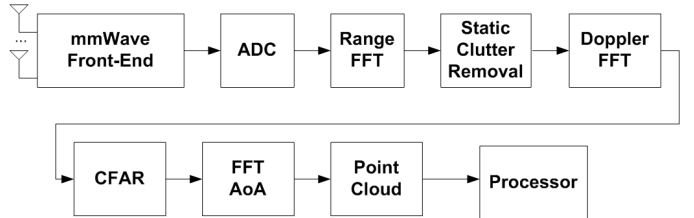
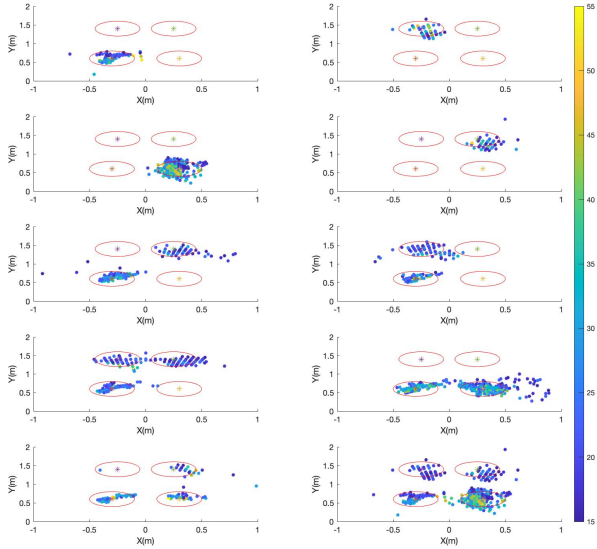


Fig. 6. Mmwave radar processing chain.

#### IV. SEAT OCCUPANCY ALGORITHM

Figures 7 and 8 show the point cloud and the measured SNR for each point during 10 seconds in a car with 4 and 5 seats, respectively. Based on these plots, an algorithm has been developed for classification from some features.

Firstly, some parameters have been defined to roughly determine the seating areas shown in red in figures 7 and 8. The area of space occupied by a body approximates that of an ellipsoid. These ellipsoids are referenced to the coordinates of the center of the interior of the vehicle ( $X_k, Y_k$ ) and the radius in horizontal ( $R_{xk}$ ) and in vertical ( $R_{yk}$ ), where  $k$  is the index of seat,  $k = 1 \dots N_{seats}$ . These parameters are the input of the algorithm and can vary depending on the car. However, they can be obtained from a table as a function of the vehicle



**Fig. 7.** Point cloud measured for a four-seater car depending on the seat. The colored bar shows the measured SNR. The seating areas are marked in red.

model or specified manually by the user. As example, Table II provides the values that define the seating areas for two cars with 4 and 5 seats.

The algorithm takes into account the points cloud saved over a period of time. Once the regions of every point have been calculated, their coordinates are saved in the vectors  $\bar{X}_k$  and  $\bar{Y}_k$ . A point  $(x_i, y_i)$  is in zone  $k$  if it belongs to the ellipsoid:

$$\sqrt{\left(\frac{x_i - X_{Ck}}{R_{xk}}\right)^2 + \left(\frac{y_i - Y_{Ck}}{R_{yk}}\right)^2} < 1 \quad (7)$$

where  $X_{Ck}$  and  $Y_{Ck}$  are the coordinates of the center of the area  $k$ , and  $R_{xk}$  and  $R_{yk}$  are the semi-axes of the ellipsoid in the directions  $x$  and  $y$ , respectively.

Then the number of the point  $N_k$  of the cloud that belongs to a specific area is the length of vector  $\bar{X}_k$  or  $\bar{Y}_k$ .

The mobility of a seated person produces a dispersion of the points in each occupied seat. The standard deviation of the points in each zone gives a measure of this dispersion:

$$\sigma_k = \sqrt{\frac{1}{N_k} \sum_{i=1}^{i=N_k} (X_{ki} - E(\bar{X}_k))^2 + (Y_{ki} - E(\bar{Y}_k))^2} \quad (8)$$

where  $E()$  denotes the mean operator and  $X_{ki}$  and  $Y_{ki}$  are the components of the vectors  $\bar{X}_k$  or  $\bar{Y}_k$ , respectively. The following classification function is defined:

$$f_k = \frac{\sigma_k \cdot \frac{N_k}{N}}{\sum_{k=1}^{N_z} \sigma_k \cdot \frac{N_k}{N}} \quad (9)$$

This normalized function corresponds to the standard deviation of the points in each zone ( $\sigma_k$ ) multiplied by the density of points in the zone ( $N_k/N$ ). The function includes the fraction of points to avoid false detection when a seat is empty,

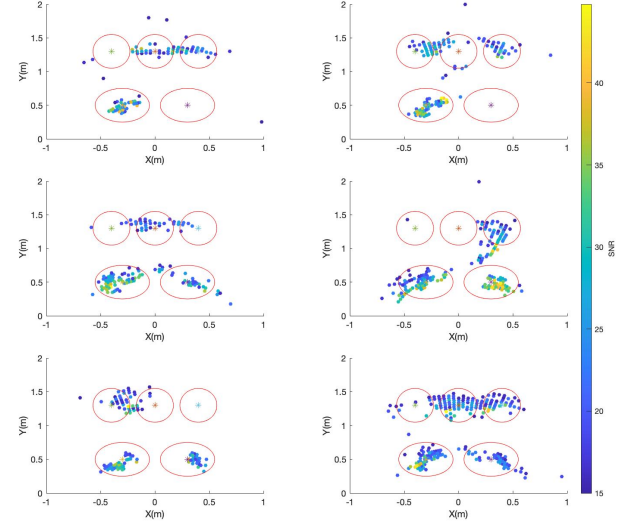


**Fig. 8.** Point cloud measured for a five-seater car depending on the seat. The colored bar shows the measured SNR. The seating areas are marked in red.

characterized by a small number of points read by the radar, sometimes dispersed due to residual clutter. A threshold is established for each zone,  $TH_k$ . If  $f_k > TH_k$  the seat is considered occupied. The seat state (0 or 1) is saved in a vector  $so_k$ .

$$so_k[n] = \begin{cases} 1 & , f_k[n] > TH_k \\ 0 & , \text{else} \end{cases} \quad (10)$$

The threshold value varies between the front and rear seats due that for certain blockage the number of points in the rear regions has been observed smaller than for the front zones. The threshold values are fixed and are obtained from the typical values obtained for the function  $f_k$  from sets of measurements. The values obtained are listed in Table II.

Finally, the seat occupancy vector is averaged to eliminate errors associated with passenger movement (eg. when entering or exiting the vehicle). A moving average filter is used (eg. by averaging the last  $M=3$  samples) and the result is compared to a threshold ( $m=0.5$ ). The filtered seat occupancy  $\bar{so}_k$  is obtained from:

$$\bar{so}_k[n] = \begin{cases} 1 & , \frac{1}{M} \sum_{i=n-M+1}^n so_k[i] > m \\ 0 & , \text{else} \end{cases} \quad (11)$$

where  $so_k$  is the seat occupancy for seat  $k$ th.

Figure 9 shows the flow chart of the algorithm. The algorithm has been implemented in both Matlab and Python. The latter allows to run the algorithm on different platforms including Raspberry Pi platforms.

## V. RESULTS

First, the acquisition radar algorithms have been tested to distinguish between people and objects that may occupy the seats. Figure 10 shows the point cloud measured in a car occupied by the driver and a bag in one of the side seats. It

**TABLE II**  
GEOMETRIC PARAMETERS ACCORDING TO THE NUMBER OF SEATS IN  
THE VEHICLE

Parameter	4 seats	5 seats
Distance radar to front seat row	60 cm	50 cm
Distance between front seats	60 cm	60 cm
Distance between back seats	60 cm	80 cm
Distance between front and back seats	80 cm	80 cm
Horizontal semi-axis front seats	20 cm	25 cm
Horizontal semi-axis back seats	20 cm	17 cm
Vertical semi-axis front seats	20 cm	20 cm
Vertical semi-axis back seats	20 cm	20 cm
Threshold (TH) for front seats	0.01	0.01
Threshold (TH) for back seats	0.005	0.05

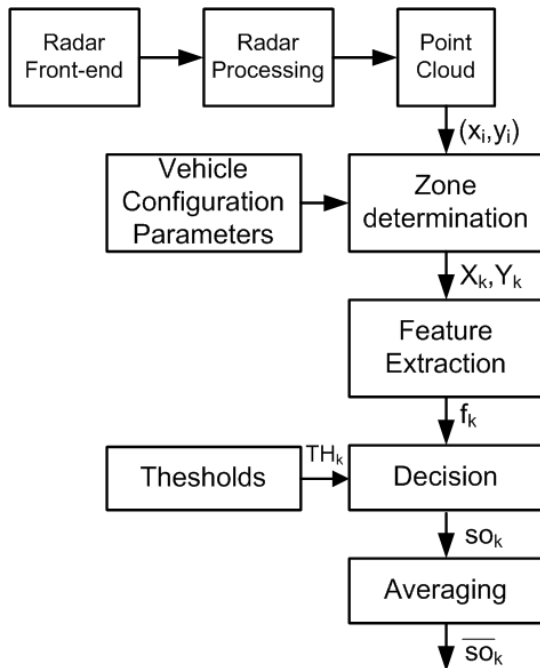


Fig. 9. Processing chain flow diagram.

can be seen that there are practically no points on the seat on which the bag is located. Another test was performed to show that vehicle movement does not significantly affect detection. Figure 11 shows the results obtained; it can be observed that the cloud does not vary hardly with respect to the static case (i.e. the one shown in Figure 10). Secondly, different people sat in a vehicle in any of the seats at random, and the positions of the occupied seats were recorded manually and compared with the predictions given by the classification algorithm. The confusion matrices of the number of occupants obtained for the case of a 4 and 5-seat vehicle are shown in Figures 12 and 13, respectively. In the confusion matrix plot, the rows are the predicted class (Output Class) and the columns the true class (Target Class). A row summary shows the percentages of correctly and incorrectly classified observations for each true class. Similarly, a column summary shows the percentages of correctly and incorrectly classified observations for each predicted class. The accuracy found is 96% and 90% for 4- and 5-seats, respectively. The lower value obtained in the case of 5 seats is explained by the greater difficulty to distinguish the rear seats because the distance between seats is less than

in the 4-seater car.

In order to investigate the error in the prediction of the correct seat, Fig. 14 shows the confusion matrix of the state of each seat for the case of 4-seater car. The classes have been coded in binary (0001 seat number 1 occupied and 1111 for all seats occupied) It can be seen that most of the errors occur in the rear seats where the seating position is not as well defined as in the front ones. Even so, the error obtained is acceptable (accuracy of 86.125%), especially if the occupancy rate can be averaged over time, which will not vary as long as an occupant does not enter or exit the vehicle.

The proposed algorithm has low computational load, therefore it can be implemented in real time, allowing the occupation to be dynamically updated. Fig. 15 shows an example of occupancy detection (0 free, 1 occupied) of each seat in a 4-seat car, as a function of the time and as passengers enter or exit the vehicle. Some isolated errors can be observed when the passengers enter or exit from the vehicle. However the algorithm detects the seat occupancy when the position remains stable, indicated with red rectangles. These failed points associated with transitions could be removed using the moving average filter provided in (11).

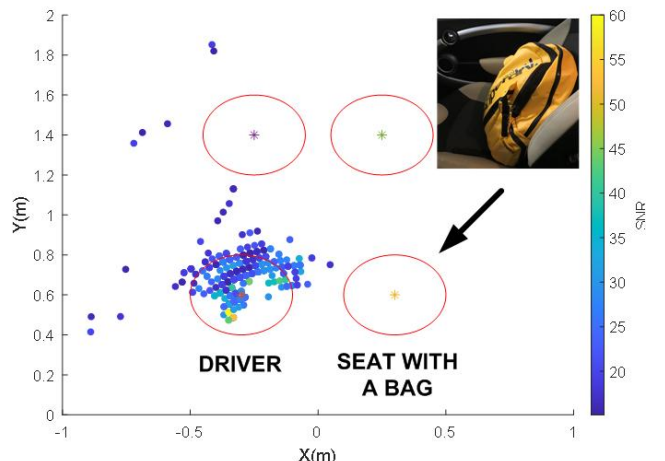
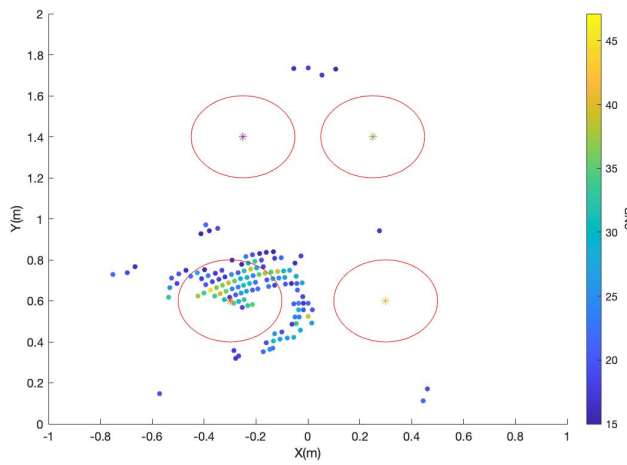


Fig. 10. Point cloud measured with the driver present and a bag (inset figure) occupying the passenger seat.

## VI. CONCLUSION AND FUTURE WORK

A vehicle occupancy detection system based on a MIMO FMCW mmWave radar at 77 GHz has been investigated. The radar is suspended on the ceiling of the vehicle, although it can also be in other places where it has visibility of the passengers. An algorithm to determine the seat occupancy from the measured point cloud read by the radar has been proposed. A static clutter removal algorithm is applied to consider only points associated to small body movements. Therefore, the system is able to detect and distinguish a passenger from other objects that may occupy the seat. A classification method is used, which is based on a function that takes into account the dispersion of the point cloud around the area in which the seat is located, as well as the point density of the cloud. Therefore, complex learning tools that require



**Fig. 11.** Point cloud measured with the driver present and the car in motion.

Confusion Matrix for Validation Data						
True Class	Predicted Class					Percentage
	0	1	2	3	4	
0	20					100.0%
1		18	2			90.0% 10.0%
2			20			100.0%
3			1	19		95.0% 5.0%
4			1	19		95.0% 5.0%
	100.0%	100.0%	87.0%	95.0%	100.0%	
			13.0%	5.0%		

**Fig. 12.** Confusion matrix of the number of occupants for the case of a 4-seater car.

training procedures are not needed. Experimental results have been presented for 4 and 5-seater cars achieving high accuracy both in determining the number of occupants and the position of the occupied seat. This work opens the door to use the proposed occupancy detector combined with future vehicular communications systems, to apply it, for instance, to high-occupancy-vehicle (HOV) lanes.

## REFERENCES

- [1] J. Lee, J. Byun, J. Lim, and J. Lee, "A framework for detecting vehicle occupancy based on the occupant labeling method," *Journal of Advanced Transportation*, vol. 2020, 2020.
- [2] A. Lazaro, M. Lazaro, R. Villarino, and D. Girbau, "Seat-occupancy detection system and breathing rate monitoring based on a low-cost mm-wave radar at 60 GHz," *IEEE Access*, 2021.
- [3] B. Alefs, M. Clabian, H. Bischof, W. Kropatsch, and F. Khairallah, "Robust occupancy detection from stereo images," in *Proceedings. The 7th International IEEE Conference on Intelligent Transportation Systems (IEEE Cat. No. 04TH8749)*. IEEE, 2004, pp. 1–6.
- [4] M. Deruyter and K. Anckaert, "Video-based parking occupancy detection," in *Video Surveillance and Transportation Imaging Applications*, vol. 8663. International Society for Optics and Photonics, 2013, p. 866300.
- [5] B. Xu, P. Paul, Y. Artan, and F. Peronnin, "A machine learning approach to vehicle occupancy detection," in *17th International IEEE Conference on Intelligent Transportation Systems (ITSC)*. IEEE, 2014, pp. 1232–1237.
- [6] B. Balci, B. Alkan, A. Elihos, and Y. Artan, "Front seat child occupancy detection using road surveillance camera images," in *2018 25th IEEE*

Confusion Matrix for Validation Data						
True Class	Predicted Class					Percentage
	0	1	2	3	4	
0	20					100.0%
1		19	1			95.0% 5.0%
2		1	18	1		90.0% 10.0%
3				18	2	90.0% 10.0%
4			1	2	17	85.0% 15.0%
5				2	2	80.0% 20.0%
	100.0%	95.0%	90.0%	78.3%	81.0%	100.0%
		5.0%	10.0%	21.7%	19.0%	

**Fig. 13.** Confusion matrix of the number of occupants for the case of a 5-seater car.

Confusion Matrix for Validation Data																
True Class	Predicted Class															Percentage
	0	1	2	3	4	5	6	7	8	9	10	11	12	13	14	15
0	10															100.0%
1		9	1													90.0% 10.0%
2			8													80.0% 20.0%
3				10												100.0%
4			1		8											86.0% 20.0%
5					7											70.0% 30.0%
6						10										100.0%
7							7									70.0% 30.0%
8								3								100.0%
9									1							70.0% 30.0%
10										1						100.0%
11											7					90.0% 10.0%
12												10				100.0%
13													9			90.0% 10.0%
14													2			90.0% 10.0%
15														6		60.0% 40.0%
	100.0%	100.0%	80.0%	90.9%	80.0%	77.8%	83.3%	58.3%	90.0%	75.0%	77.8%	90.9%	100.0%	81.8%	100.0%	100.0%
		20.0%	9.1%	20.0%	22.2%	16.7%	41.7%	10.0%	25.0%	22.2%	9.1%					18.2%

**Fig. 14.** Confusion matrix of seat occupancy status for a 4-seater car.

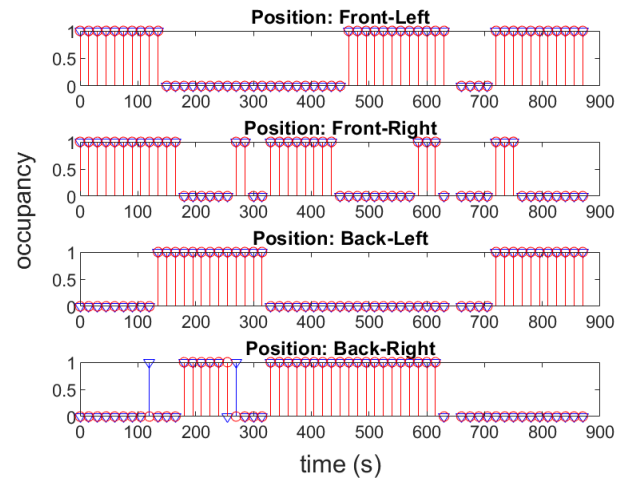


**Fig. 15.** Seat occupancy as a function of time. Marked with circles, not smoothed and with triangles, smoothed.

- International Conference on Image Processing (ICIP)*. IEEE, 2018, pp. 1927–1931.
- [7] A. Kumar, A. Gupta, B. Santra, K. Lalitha, M. Kolla, M. Gupta, and R. Singh, “VPDS: an AI-based automated vehicle occupancy and violation detection system,” in *Proceedings of the AAAI Conference on Artificial Intelligence*, vol. 33, no. 01, 2019, pp. 9498–9503.
- [8] M. Vamsi and K. Soman, “In-vehicle occupancy detection and classification using machine learning,” in *2020 11th International Conference on Computing, Communication and Networking Technologies (ICCCNT)*. IEEE, 2020, pp. 1–6.
- [9] J. Lee, D. Lee, S. Jang, D. Choi, and J. Jang, “Analysis of deep learning model for the development of an optimized vehicle occupancy detection system,” *Journal of the Korea Institute of Information and Communication Engineering*, vol. 25, no. 1, pp. 146–151, 2021.
- [10] F. Erik Nowruzi, W. A. El Ahmar, R. Laganiere, and A. H. Ghods, “In-vehicle occupancy detection with convolutional networks on thermal images,” in *Proceedings of the IEEE/CVF Conference on Computer Vision and Pattern Recognition Workshops*, 2019, pp. 0–0.
- [11] V. Padi, H. Fleyeh, and R. G. Nyberg, “Deep learning-based vehicle occupancy detection in an open parking lot using thermal camera,” *IET Intelligent Transport Systems*, vol. 14, no. 10, pp. 1295–1302, 2020.
- [12] A. Makrushin, M. Langnickel, M. Schott, C. Vielhauer, J. Dittmann, and K. Seifert, “Car-seat occupancy detection using a monocular 360° nir camera and advanced template matching,” in *2009 16th International Conference on Digital Signal Processing*. IEEE, 2009, pp. 1–6.
- [13] B. Silva, P. Martins, and J. Batista, “Vehicle Occupancy Detection for HOV/HOT Lanes Enforcement,” in *2019 IEEE Intelligent Transportation Systems Conference (ITSC)*. IEEE, 2019, pp. 311–318.
- [14] J. W. Melvin, “Injury assessment reference values for the CRABI 6-month infant dummy in a rear-facing infant restraint with airbag deployment,” *SAE transactions*, pp. 1553–1564, 1995.
- [15] A. Voisin, S. Bombardier, E. Levrat, and J. Bremont, “Sensory features measurement of the under-thigh length of car seat,” in *1998 IEEE International Conference on Fuzzy Systems Proceedings. IEEE World Congress on Computational Intelligence (Cat. No. 98CH36228)*, vol. 2. IEEE, 1998, pp. 1589–1594.
- [16] K. Kasten, A. Stratmann, M. Munz, K. Dirscherl, and S. Lamers, “IBolt technology—A weight sensing system for advanced passenger safety,” in *Advanced Microsystems for Automotive Applications 2006*. Springer, 2006, pp. 171–186.
- [17] B. George, H. Zangl, T. Bretterklaiber, and G. Brasseur, “Seat occupancy detection based on capacitive sensing,” *IEEE Transactions on Instrumentation and Measurement*, vol. 58, no. 5, pp. 1487–1494, 2009.
- [18] D. Tumpold and A. Satz, “Contactless seat occupation detection system based on electric field sensing,” in *2009 35th Annual Conference of IEEE Industrial Electronics*. IEEE, 2009, pp. 1823–1828.
- [19] M. Walter, B. Eilebrecht, T. Wartzek, and S. Leonhardt, “The smart car seat: personalized monitoring of vital signs in automotive applications,” *Personal and Ubiquitous Computing*, vol. 15, no. 7, pp. 707–715, 2011.
- [20] M. Devy, A. Giralt, and A. Marin-Hernandez, “Detection and classification of passenger seat occupancy using stereovision,” in *Proceedings of the IEEE Intelligent Vehicles Symposium 2000 (Cat. No. 00TH8511)*. IEEE, 2000, pp. 714–719.
- [21] S. Wender and O. Loehlein, “A cascade detector approach applied to vehicle occupant monitoring with an omni-directional camera,” in *IEEE Intelligent Vehicles Symposium, 2004*. IEEE, 2004, pp. 345–350.
- [22] M. Mateu-Mateus, F. Guede-Fernández, N. Rodríguez-Ibáñez, M. García-González, J. Ramos-Castro, and M. Fernández-Chimeno, “A non-contact camera-based method for respiratory rhythm extraction,” *Biomedical Signal Processing and Control*, vol. 66, p. 102443, 2021.
- [23] M. Fritzsche, C. Prestele, G. Becker, M. Castillo-Franco, and B. Mirbach, “Vehicle occupancy monitoring with optical range-sensors,” in *IEEE Intelligent Vehicles Symposium, 2004*. IEEE, 2004, pp. 90–94.
- [24] G. Naik, B. Choudhury, and J.-M. Park, “Ieee 802.11 bd & 5g nr v2x: Evolution of radio access technologies for v2x communications,” *IEEE access*, vol. 7, pp. 70 169–70 184, 2019.
- [25] A. Lazaro, D. Girbau, and R. Villarino, “Analysis of vital signs monitoring using an IR-UWB radar,” *Progress In Electromagnetics Research*, vol. 100, pp. 265–284, 2010.
- [26] A. Lazaro, D. Girbau, and R. Villarino, “Techniques for clutter suppression in the presence of body movements during the detection of respiratory activity through UWB radars,” *Sensors*, vol. 14, no. 2, pp. 2595–2618, 2014.
- [27] F. Khan and S. H. Cho, “A detailed algorithm for vital sign monitoring of a stationary/non-stationary human through IR-UWB radar,” *Sensors*, vol. 17, no. 2, p. 290, 2017.
- [28] C. Li, J. Cummings, J. Lam, E. Graves, and W. Wu, “Radar remote monitoring of vital signs,” *IEEE Microwave Magazine*, vol. 10, no. 1, pp. 47–56, 2009.
- [29] D. Girbau, A. Lazaro, A. Ramos, and R. Villarino, “Remote sensing of vital signs using a doppler radar and diversity to overcome null detection,” *IEEE Sensors Journal*, vol. 12, no. 3, pp. 512–518, 2011.
- [30] C. Li, V. M. Lubecke, O. Boric-Lubecke, and J. Lin, “A review on recent advances in Doppler radar sensors for noncontact healthcare monitoring,” *IEEE Transactions on microwave theory and techniques*, vol. 61, no. 5, pp. 2046–2060, 2013.
- [31] H. Lee, B.-H. Kim, J.-K. Park, and J.-G. Yook, “A novel vital-sign sensing algorithm for multiple subjects based on 24-GHz FMCW Doppler radar,” *Remote Sensing*, vol. 11, no. 10, p. 1237, 2019.
- [32] M. Hoffmann, D. Tatarinov, J. Landwehr, and A. Diewald, “A four-channel radar system for rear seat occupancy detection in the 24 GHz ISM band,” in *2018 11th German Microwave Conference (GeMiC)*. IEEE, 2018, pp. 95–98.
- [33] M. Alizadeh, H. Abedi, and G. Shaker, “Low-cost low-power in-vehicle occupant detection with mm-wave FMCW radar,” in *2019 IEEE SENSORS*. IEEE, 2019, pp. 1–4.
- [34] Y. Ma, Y. Zeng, and V. Jain, “CarOSense: Car Occupancy Sensing with the Ultra-Wideband Keyless Infrastructure,” *Proceedings of the ACM on Interactive, Mobile, Wearable and Ubiquitous Technologies*, vol. 4, no. 3, pp. 1–28, 2020.
- [35] *AWR1642 Single-Chip 77- and 79-GHz FMCW Radar sensor*, Texas Instruments, April 2020.
- [36] *AWR1642 Evaluation Module (AWR1642BOOST) Single-Chip mmWave Sensing Solution*, Texas Instruments, May 2020.
- [37] B. Kim, S. Kim, and J. Lee, “A novel dft-based doa estimation by a virtual array extension using simple multiplications for fmcw radar,” *Sensors*, vol. 18, no. 5, p. 1560, 2018.
- [38] *MMWAVE SDK User Guide*, Texas Instruments, Sept 2020, rev. 3.5.
- [39] A. Melebari, A. K. Mishra, and M. A. Gaffar, “Comparison of square law, linear and bessel detectors for CA and OS CFAR algorithms,” in *2015 IEEE Radar Conference*. IEEE, 2015, pp. 383–388.
- [40] M. A. Habib, M. Barkat, B. Aissa, and T. Denidni, “Ca-cfar detection performance of radar targets embedded in “non centered chi-2 gamma” clutter,” *Progress In Electromagnetics Research*, vol. 88, pp. 135–148, 2008.
- [41] M. Kronauge and H. Rohling, “Fast two-dimensional CFAR procedure,” *IEEE Transactions on Aerospace and Electronic Systems*, vol. 49, no. 3, pp. 1817–1823, 2013.
- [42] M. A. Abou-Khousa, D. L. Simms, S. Kharkovsky, and R. Zoughi, “High-resolution short-range wideband fmcw radar measurements based on music algorithm,” in *2009 IEEE Instrumentation and Measurement Technology Conference*. IEEE, 2009, pp. 498–501.
- [43] C.-B. Ko and J.-H. Lee, “Performance of ESPRIT and root-MUSIC for angle-of-arrival (AOA) estimation,” in *2018 IEEE World Symposium on Communication Engineering (WSCE)*. IEEE, 2018, pp. 49–53.
- [44] P. Stoica, Z. Wang, and J. Li, “Extended derivations of MUSIC in the presence of steering vector errors,” *IEEE transactions on signal processing*, vol. 53, no. 3, pp. 1209–1211, 2005.
- [45] Stoica, P. and Zhisong Wang and Jian Li, “Robust capon beamforming,” in *Conference Record of the Thirty-Sixth Asilomar Conference on Signals, Systems and Computers*, 2002., vol. 1, 2002, pp. 876–880 vol.1.



**Nil Munte** was born in Riudoms, Spain, 1999. He received the BS in Telecommunications Engineering from Universitat Rovira i Virgili (URV) in Tarragona, Spain, in 2021. Currently, he is working as a Researcher and a part-time Associate Professor at Universitat Rovira i Virgili (URV). His research interests focus on RADAR technologies, data adquisition and data processing.



**Antonio Lázaro** (M'07–SM'16) was born in Lleida, Spain, in 1971. He received the M.S. and Ph.D. degrees in telecommunication engineering from the Universitat Politècnica de Catalunya (UPC), Barcelona, Spain, in 1994 and 1998, respectively. He then joined the faculty of UPC, where he currently teaches a course on microwave circuits and antennas. Since July 2004, he is a Full-Time Professor at the Department of Electronic Engineering, Universitat Rovira i Virgili (URV), Tarragona, Spain. His research interests are microwave device modeling, on-wafer noise measurements, monolithic microwave integrated circuits (MMICs), low phase noise oscillators, MEMS, RFID, UWB and microwave systems.



**Ramon Villarino** was awarded a degree in Telecommunications Technical Engineering by Ramon Llull University (URL) in Barcelona, Spain, in 1994, a degree in Senior Telecommunications Engineering by the Universitat Politècnica de Catalunya (UPC) in Barcelona, Spain, in 2000 and a doctorate by the UPC in 2004. In 2005-2006, he was a Research Associate at the Technological Telecommunications Center of Catalonia (CTTC) in Barcelona, Spain. He worked as a Researcher and Assistant Professor at the Universitat Autònoma de Barcelona (UAB) from 2006 to 2008. Since January 2009 he has been a full-time professor at Universitat Rovira i Virgili (URV) in Tarragona, Spain. His research activities focus on radiometry, microwave devices, and systems based on UWB, RFIDs, and frequency selective structures using MetaMaterials (MM).



**David Girbau** (M'04–SM'13) was awarded a BSc in Telecommunication Engineering, a MSc in Electronics Engineering, and a doctorate in Telecommunication by Universitat Politècnica de Catalunya (UPC) in Barcelona, Spain, in 1998, 2002 and 2006, respectively. From February 2001 to September 2007 he was a Research Assistant at UPC. From September 2005 to September 2007 he was a part-time Assistant Professor at Universitat Autònoma de Barcelona (UAB). Since October 2007 he has been a full-time professor at Universitat Rovira i Virgili (URV) in Tarragona, Spain. His research interests include microwave devices and systems, with an emphasis on UWB, RFIDs, RF-MEMS and wireless sensors.